Available online at www.sciencedirect.com
SCIENCE DIRECT®
Biochemical and Biophysical Research Communications 309 (2003) 917–922
BBRC
www.elsevier.com/locate/ybbrc

Structural basis for inhibition of human PNP by immucillin-H

Walter Filgueira de Azevedo Jr.,[a,b,*] Fernanda Canduri,[a,b] Denis Marangoni dos Santos,[a,b] José Henrique Pereira,[a,b] Márcio Vinicius Bertacine Dias,[a] Rafael Guimarães Silva,[c] Maria Anita Mendes,[b,d] Luiz Augusto Basso,[c] Mário Sérgio Palma,[b,d] and Diógenes Santiago Santos[c,e,*]

[a] *Departamento de Física, UNESP, São José do Rio Preto, SP 15054-000, Brazil*
[b] *Center for Applied Toxinology, Instituto Butantan, São Paulo, SP 05503-900, Brazil*
[c] *Rede Brasileira de Pesquisas em Tuberculose., Departamento de Biologia Molecular e Biotecnologia, UFRGS, Porto Alegre, RS 91501-970, Brazil*
[d] *Laboratory of Structural Biology and Zoochemistry-CEIS, Department of Biology, Institute of Biosciences UNESP, Rio Claro, SP 13506-900, Brazil*
[e] *Faculdade de Farmácia, Instituto de Pesquisas Biomédicas, Pontifícia Universidade Católica do Rio Grande do Sul, Porto Alegre, RS, Brazil*

Received 19 August 2003

Abstract

Purine nucleoside phosphorylase (PNP) catalyzes the phosphorolysis of the *N*-ribosidic bonds of purine nucleosides and deoxynucleosides. PNP is a target for inhibitor development aiming at T-cell immune response modulation. This work reports on the crystallographic study of the complex of human PNP–immucillin-H (HsPNP–ImmH) solved at 2.6 Å resolution using synchrotron radiation. Immucillin-H (ImmH) inhibits the growth of malignant T-cell lines in the presence of deoxyguanosine without affecting non-T-cell tumor lines. ImmH inhibits activated normal human T cells after antigenic stimulation in vitro. These biological effects of ImmH suggest that this agent may have utility in the treatment of certain human diseases characterized by abnormal T-cell growth or activation. This is the first structural report of human PNP complexed with immucillin-H. The comparison of the complex HsPNP–ImmH with recent crystallographic structures of human PNP explains the high specificity of immucillin-H for human PNP.

Keywords: PNP; Synchrotron radiation; Structure; Immucillin-H; Drug design

Mutations in the locus encoding for purine nucleoside phosphorylase (PNP) cause gradual decrease in T-cell immunity, though keeping B-cell immunity normal as well as other tissues [1]. The activation of helper T cells requires that they recognize a complex formed between an antigen and a class II MHC protein on the surface of antigen-presenting cells with appropriate costimulation. This results in interleukin-2 release which, in turn, leads to T-cell clonal expansion with activity against cells exhibiting the stimulatory antigen [2]. However, most naive T-cells receive no antigenic signal and undergo apoptosis. Cellular nucleic acids from the apoptosed cells are recycled. Naive T-cells have the ability to transport and phosphorylate deoxyguanosine to dGTP, which accumulates relative to normal cells [3]. One proposal is that the absence of PNP activity leads to the accumulation of deoxyguanosine triphosphate, which inhibits the enzyme ribonucleotide reductase and ensuing DNA synthesis inhibition, thereby preventing cellular proliferation required for an immune response [4]. Thus, this enzyme is a potential target for drug development, which could induce immune suppression to treat, for instance, autoimmune diseases, T-cell leukemia and lymphoma, and organ transplantation rejection [5]. Accordingly, a transition-state analog (immucillin-H) (Fig. 1) that inhibits PNP enzyme activity has recently been shown to inhibit the growth of malignant T-cell leukemia cell lines with the induction of apoptosis [6]. In addition, some PNP inhibitors have been tested in combination with nucleoside antiviral and anticancer drugs showing

* Corresponding authors. Fax: +55-17-221-2247 (W. Filgueira de Azevedo).
E-mail address: walterfa@df.ibilce.unesp.br (W. Filgueira de Azevedo Jr.).

0006-291X/$ - see front matter © 2003 Elsevier Inc. All rights reserved.
doi:10.1016/j.bbrc.2003.08.094

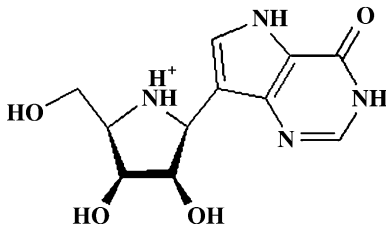

Fig. 1. Molecular structure of immucillin-H [(1S)-1-(9-deazahypoxanthin-9-yl)-1,4-dideoxy-1,4-imino-D-ribitol].

the ability to potentiate the in vivo activity of these drugs [7].

PNP catalyzes the reversible phosphorolysis of *N*-ribosidic bonds of both purine nucleosides and deoxynucleosides, except adenosine, generating purine base and ribose (or deoxyribose) 1-phosphate [8]. The major physiological substrates for mammalian PNP are inosine, guanosine, and 2′-deoxyguanosine [9]. PNP is specific for purine nucleosides in the β-configuration and exhibits a preference for ribosyl-containing nucleosides relative to the analogs containing the arabinose, xylose, and lyxose stereoisomers [10]. Moreover, PNP cleaves glycosidic bond with inversion of configuration to produce α-ribose 1-phosphate, as shown by its catalytic mechanism [11].

We have obtained the crystallographic structure of the complex between HsPNP and immucillin-H (HsPNP–ImmH). To the best of our knowledge, this is the first structural report of the complex between human PNP and immucillin-H. Our analyses of the HsPNP–ImmH structural data and structural differences between the PNP apoenzyme and HsPNP–ImmH complex provide explanation for substrate binding, refine the purine-binding site, and can be used for future inhibitor design.

Materials and methods

Crystallization and data collection. Recombinant human PNP was expressed and purified as previously described [12]. HsPNP–ImmH was crystallized using the experimental conditions described elsewhere [13,14]. In brief, a PNP solution was concentrated to 13 mg mL^{-1} against 10 mM potassium phosphate buffer (pH 7.1) and incubated in the presence of 0.6 mM immucillin-H (a gift from BioCryst Pharmaceuticals, Birmingham, AL, USA). Hanging drops were equilibrated by vapor diffusion at 25 °C against a reservoir containing 19% saturated ammonium sulfate solution in 0.05 M citrate buffer (pH 5.3).

In order to increase the resolution of the HsPNP–ImmH crystal, we collected data from a flash-cooled crystal at 104 K. Prior to flash cooling, glycerol was added, up to 50% by volume, to the crystallization drop. X-ray diffraction data were collected at a wavelength of 1.4310 Å using the Synchrotron Radiation Source (Station PCr, Laboratório Nacional de Luz Síncrotron, LNLS, Campinas, Brazil) and a CCD detector (MARCCD) with an exposure time of 30 s per image at a crystal to detector distance of 120 mm. X-ray diffraction data were processed to 2.6 Å resolution using the program MOSFLM and scaled with the program SCALA [15].

Upon cooling the cell parameters shrank from $a = b = 142.90$ Å, $c = 165.20$ Å to $a = b = 139.39$ Å, and $c = 161.31$ Å. For HsPNP–ImmH complex the volume of the unit cell is 2.714×10^6 Å^3 compatible with one monomer in the asymmetric unit with a V_m value of 4.71 Å^3 Da^{-1}. Assuming a value of 0.26 cm^3 g^{-1} for the protein partial

Table 1
Data collection and refinement statistics

Cell parameters	$a = b = 139.39$ Å, $c = 161.31$ Å $\alpha = \beta = 90.00°$, $\gamma = 120.00°$
Space group	R32
Number of measurements with $I > 2\sigma(I)$	87,018
Number of independent reflections	16,705
Completeness in the range from 56.80 to 2.60 Å (%)	90.1
R_{sym}[a] (%)	9.9
Highest resolution shell (Å)	2.74–2.60
Completeness in the highest resolution shell (%)	93.4
R_{sym}[a] in the highest resolution shell (%)	37.5
Resolution range used in the refinement (Å)	7.0–2.6
R_{factor}[b] (%)	20
R_{free}[c] (%)	27.2
B values[d] (Å^2)	
Main chain	27.34
Side chains	29.96
Immucillin-H	34.83
Waters	25.11
Sulfate groups	29.28
Observed r.m.s.d from ideal geometry	
Bond lengths (Å)	0.013
Bond angles (°)	1.89
Dihedrals (°)	25.82
No. of water molecules	64
No. of sulfate groups	3

[a] $R_{sym} = 100 \sum |I(h) - \langle I(h)\rangle| / \sum I(h)$ with $I(h)$, observed intensity and $\langle I(h)\rangle$, mean intensity of reflection h over all measurement of $I(h)$.
[b] $R_{factor} = 100 \times \sum |F_{obs} - F_{calc}| / \sum (F_{obs})$, the sums being taken over all reflections with $F/\sigma(F) > 2$ cutoff.
[c] $R_{free} = R_{factor}$ for 10% of the data, which were not included during crystallographic refinement.
[d] *B* values = average *B* values for all non-hydrogen atoms.

specific volume, the calculated solvent content in the crystal is 74% and the calculated crystal density 1.09 g cm^{-3}.

Crystal structure. The crystal structure of the HsPNP–ImmH was determined by standard molecular replacement methods using the program AMoRe [16], using as search model the structure of HsPNP (PDB access code: 1M73) [17,18]. Structure refinement was performed using X-PLOR [19]. The atomic positions obtained from molecular replacement were used to initiate the crystallographic refinement. The overall stereochemical quality of the final model for HsPNP–ImmH complex was assessed by the program PROCHECK [20]. Atomic models were superposed using the program LSQKAB from CCP4 [15].

Results and discussion

Molecular replacement and crystallographic refinement

The standard procedure of molecular replacement using AMoRe [16] was used to solve the structure. After translation function computation the correlation was of 71% and the R_{factor} of 32%. The highest magnitude of the correlation coefficient function was obtained for the Euler angles $\alpha = 114.26°$, $\beta = 58.45°$, and $\gamma = 157.79°$. The fractional coordinates are $T_x = 0.4965$, $T_y = 0.2904$, and $T_z = 0.1995$. At this stage $2F_{\text{obs}} - F_{\text{calc}}$ omit maps were calculated. These maps showed clear electron density for the immucillin-H in the complex. Further refinement in X-PLOR continued with simulated annealing using the slow-cooling protocol, followed by alternate cycles of positional refinement and manual rebuilding using XtalView [21]. Finally, the positions of immucillin-H, water, and sulfate molecules were checked and corrected in $F_{\text{obs}} - F_{\text{calc}}$ maps. The final model has an R_{factor} of 20.0% and an R_{free} of 27.2%, with 64 water molecules, three sulfate ions, and the immucillin-H.

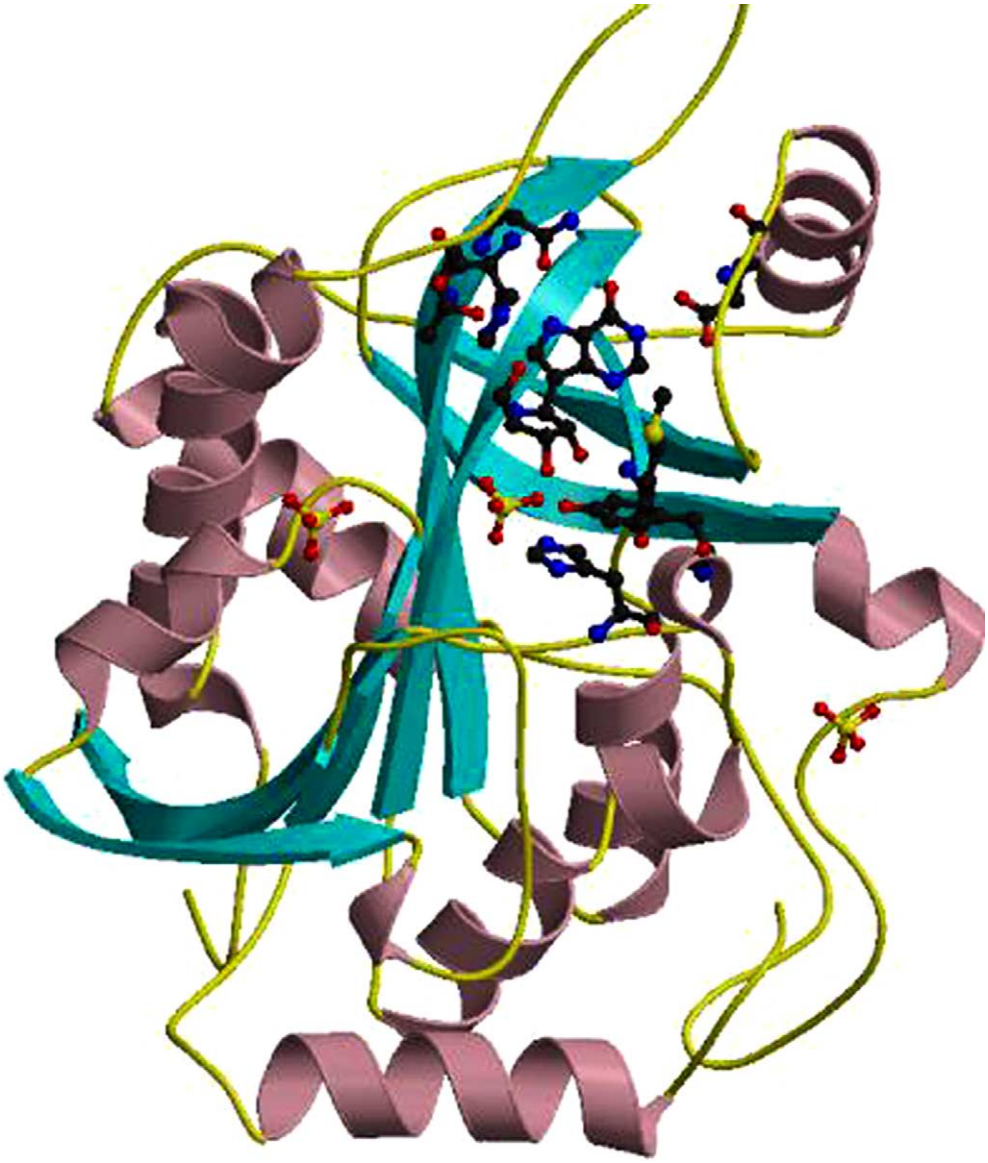

Fig. 2. Ribbon diagram of HsPNP–ImmH generated by Molscript [40] and Raster3d [41].

Ignoring low-resolution data, a Luzzati plot [22] gives the best correlation between the observed and calculated data for a predicted mean coordinate error of 0.29 Å. The average *B* factor for main chain atoms is 27.34 Å^2, whereas that for side chain atoms is 29.96 Å^2. *B* factors for water molecules range from 13.23 to 58.87 Å^2, with an average of 25.11 Å^2 and the average *B* factor for immucillin-H molecule is 34.83 Å^2 (Table 1).

Overall description

Analysis of the crystallographic structure of HsPNP–ImmH complex indicates a trimeric structure. Each PNP monomer displays an α/β-fold consisting of a mixed β-sheet surrounded by α helices. The structure contains an eight-stranded mixed β-sheet and a five-stranded mixed β-sheet, which join to form a distorted β-barrel. Fig. 2 shows schematic drawings of the PNP–ImmH complex.

Ligand-binding conformational changes

There is a conformational change in the PNP structure when immucillin-H binds in the active site. The overall change is relatively small, with an r.m.s.d. in the coordinates of all Cα of 1.2 Å after superimposition of PNP apoenzyme onto HsPNP–ImmH complex.

Particularly interesting is the position occupied by the Lys244 in the present complex structure and in the human PNP (1M73) [17]. The hydrogen bond between the Lys244NZ and O6 of the purine ring was previously predicted from molecular modeling studies [23], since electron density was not detected for the Lys244 side-chain atoms in the low-resolution PNP structures [14,24]. The structure of complex HsPNP–ImmH, here described, presents clear electron density for the Lys244 region. The ε-amino group of Lys244 forms hydrogen bond with the carbonyl group of Asn121 (2.77 Å), in the present structure, indicating that the side-chain of Lys244 is firmly locked in this region. Similar positioning for Lys244 is observed in the high-resolution structures of bovine PNP [25,26] and in the high-resolution structure of HsPNP (1M73). Furthermore, the same region of the complex between HsPNP and immucillin-H indicates small movement of the Lys244 side chain. Analysis of the same region in the low-resolution structure of HsPNP complexed with guanine (PDB access code: 1ULB) indicates a large movement in the Lys244 side chain upon binding of guanine, suggesting that the ε-amino group of Lys244 in the HsPNP moves 9.1 Å upon guanine binding.

Interactions with immucillin-H

The specificity and affinity between enzyme and its inhibitor depend on directional hydrogen bonds and ionic interactions, as well as on shape complementarity of the contact surfaces of both partners [27–35]. The atomic coordinates of the HsPNP–ImmH were used for structural comparison with the complex between HsPNP and other inhibitors. We focused our analysis on three inhibitors: 8-aminoguanine, 8-amino-9-benzylguanine, and immucillin-H (trade name BCX-1777). Values of 0.8 and 0.2 μM for K_i have been determined for 8-aminoguanine and 8-amino-9-benzylguanine, respectively [36]. Immucillin-H is an inhibitor of human PNP based on the transition-state structure and exhibits slow-onset tight-binding inhibition with a rapid initial binding phase and a K_i* value of 72 pM [37]. Fig. 3 shows the intermolecular hydrogen bonds for the complex HsPNP–ImmH. Analysis of the hydrogen bonds between immucillin-H and PNP reveals eight hydrogen bonds, involving the residues His86, Tyr88, Glu201, Met219, Thr242, Asn243, and His257. It was identified only four hydrogen bonds between 8-aminoguanine and the PNP, involving the residues Ala116, Glu201, Asn243, and Lys244. For the complex between PNP and 8-amino-9-benzylguanine a total of five hydrogen bonds are observed, involving the residues Glu201, Asn243, and Lys244. However, the hydrogen bond involving ε-amino group of Lys244 is highly questionable, as discussed. Analysis of the three complexes strongly indicates that additional binding affinity, observed for

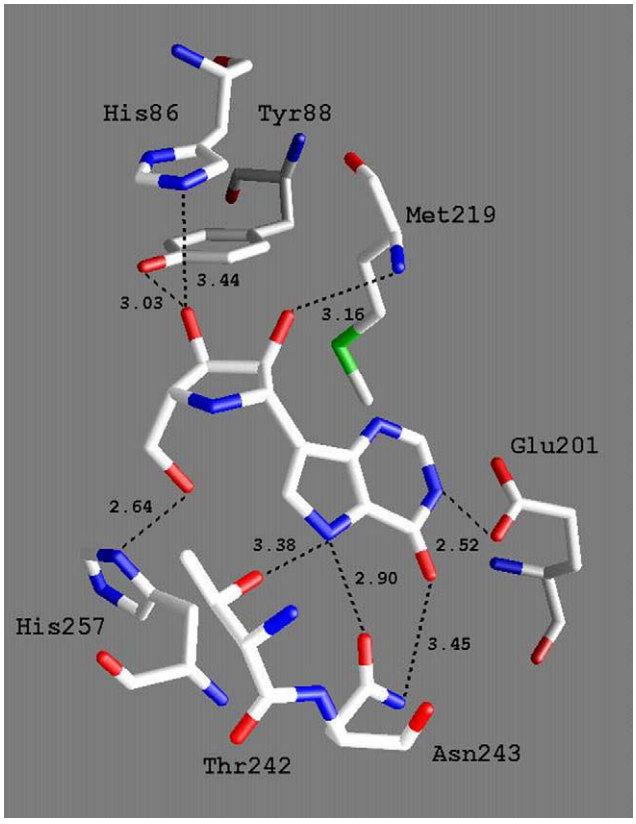

Fig. 3. Intermolecular hydrogen bonds for the complex HsPNP–Immh.

immucillin-H, may result from hydrogen bonds between O3′ and His86, and O2′ and the amide nitrogen of Met219. These results are in accordance with structural studies on bovine PNP showing that the increase in binding affinity of ImmH involves improved H-bond distances at seven or more sites in the PNP complex with ImmH relative to Michaelis complex with inosine [38]. The electrostatic potential surface of the immucillin-H complexed with HsPNP was calculated with GRASP [39] (figure not shown). The analysis of the charge distribution of the binding pockets indicates the presence of some charge complementarity between inhibitor and enzyme, though most of the binding pocket is hydrophobic.

The atomic coordinates and the structure factors for the complex HsPNP–ImmH have been deposited in the PDB with the accession code: 1PF7.

Acknowledgments

We acknowledge Dr. Shanta Bantia from Biocryst Pharmaceuticals Inc. (Birmingham, AL) for the generous gift of immucillin-H. We also acknowledge the expertise of Denise Cantarelli Machado for the expansion of the cDNA library and Deise Potrich for the DNA sequencing. This work was supported by grants from FAPESP (SMOLBNet, Proc.01/07532-0), CNPq, CAPES and Instituto do Milênio (CNPq-MCT). WFA (CNPq, 300851/98-7), MSP (CNPq, 500079/90-0), and LAB (CNPq, 520182/99-5) are researchers for the Brazilian Council for Scientific and Technological Development.

References

[1] W. Stoop, B.J.M. Zegers, G.F.M. Hendrickx, L.H.S. van Heukelom, G.E.J. Staal, P.K. de Bree, S.K. Wadman, R.E. Ballieux, Purine nucleoside phosphorylase deficiency associated with selective cellular immunodeficiency, N. Engl. J. Med. 296 (1977) 651–655.

[2] W. Levinson, E. Jawetz, Medical Microbiology and Immunology, Lange Medical Books/McGraw-Hill, New York, 2000, pp. 344–363.

[3] S. Banthia, J.A. Montgomery, H.G. Johnson, G.M. Walsh, In vivo and in vitro pharmacologic activity of the purine nucleoside phosphorylase inhibitor BCX-34: the role of GTP and dGTP, Immunopharmacology 35 (1996) 53–63.

[4] B.S. Mitchell, E. Meijias, P.E. Daddona, W.N. Kelley, Purinogenic immunodeficiency diseases: selective toxicity of deoxyribonucleosides for T-cells, Proc. Natl. Acad. Sci. USA 75 (1978) 5011–5014.

[5] J.D. Stoeckler, in: R.I. Glazer (Ed.), Developments in Cancer Chemotherapy, CRC Press, Bocca Raton, FL, 1984, pp. 35–60.

[6] G. Kicska, L. Long, H. Hörig, G. Fairchild, P.C. Tyler, R.H. Furneaux, V.L. Schramm, H.L. Kaufman, Immucillin H, a powerful transition-state analog inhibitor of purine nucleoside phosphorylase, selectively inhibits human T lymphocytes, Proc. Natl. Acad. Sci. USA 98 (2001) 4593–4598.

[7] L.L. Bennett Jr., P.W. Allan, P.E. Noker, L.M. Rose, S. Niwas, J.A. Montgomery, M.D. Erion, Purine nucleoside phosphorylase inhibitors: biochemical and pharmacological studies with 9-benzyl-9-deazaguanine and related compounds, J. Pharmacol. Exp. Ther. 266 (1993) 707–714.

[8] R.E. Parks Jr., R.P. Agarwal, in: P.D. Boyer (Ed.), The Enzymes, Academic Press, New York, 1972, pp. 483–514.

[9] V.L. Schramm, Enzymatic transition states and transition state analog design, Annu. Rev. Biochem. 67 (1998) 693–720.

[10] J.D. Stoeckler, C. Cambor, R.E. Parks Jr., Human erythrocytic purine nucleoside phosphorylase: reaction with sugar-modified nucleosides substrates, Biochemistry 19 (1980) 102–107.

[11] D.J.T. Porter, Purine nucleoside phosphorylase. Kinetic mechanism of the enzyme from calf spleen, J. Biol. Chem. 267 (1992) 7342–7351.

[12] R.G. Silva, L.P. Carvalho, J.S. Oliveira, C.A. Pinto, M.A. Mendes, M.S. Palma, L.A. Basso, D.S. Santos, Cloning, overexpression, and purification of functional human purine nucleoside phosphorylase, Protein Expr. Purif. 27 (1) (2003) 158–164.

[13] W.J. Cook, S.E. Ealick, C.E. Bugg, J.D. Stoeckler, R.E. Parks Jr., J. Biol. Chem. 256 (1981) 4079–4080.

[14] S.E. Ealick, Y.S. Babu, C.E. Bugg, M.D. Erion, W.C. Guida, J.A. Montgomery, J.A. Secrist III, Application of crystallographic and modeling methods in the design of purine nucleoside phosphorylase inhibitors, Proc. Natl. Acad. Sci. USA 91 (1991) 11540–11544.

[15] Collaborative Computational Project, No. 4. Acta Crystallogr. D 50 (1994) 760–763.

[16] J. Navaza, AMoRe: an automated package for molecular replacement, Acta Crystallogr. A 50 (1994) 157–163.

[17] W.F. De Azevedo Jr., F. Canduri, D.M. Santos, R.G. Silva, J.S. Oliveira, L.P.S. Carvalho, L.A. Basso, M.A. Mendes, M.S. Palma, D.S. Santos, Crystal structure of human purine nucleoside phosphorylase at 2.3 Å resolution, Biochem. Biophys. Res. Commun. 308 (2003) 545–552.

[18] D.M. Santos, F. Canduri, J.H. Pereira, M.V.B. Dias, R.G. Silva, M.A. Mendes, M.S. Palma, L.A. Basso, W.F. de Azevedo, D.S. Santos, Crystal structure of human purine nucleoside phosphorylase complexed with acyclovir, Biochem. Biophys. Res. Commun. 308 (2003) 553–559.

[19] A.T. Brünger, X-PLOR Version 3.1: A System for Crystallography and NMR, Yale University Press, New Haven, 1992.

[20] R.A. Laskowski, M.W. MacArthur, D.K. Smith, D.T. Jones, E.G. Hutchinson, A.L. Morris, D. Naylor, D.S. Moss, J.M. Thorton, PROCHECK v.3.0—Program to Check the Stereochemistry Quality of Protein Structures—Operating Instructions, 1994.

[21] D.E. McRee, XtalView/Xfit—a versatile program for manipulating atomic coordinates and electron density, J. Struct. Biol. 125 (1999) 156–165.

[22] P.V. Luzzati, Traitement statistique des erreurs dans la determination des structures cristallines, Acta Crystallogr. 5 (1952) 802–810.

[23] M.D. Erion, K. Takabayashi, H.B. Smith, J. Kessi, S. Wagner, S. Hönger, S.L. Shames, S.E. Ealick, Purine nucleoside phosphorylase. 1. Structure–function studies, Biochemistry 36 (1997) 11725–11734.

[24] S.E. Ealick, S.A. Rule, D.C. Carter, T.J. Greenhough, Y.S. Babu, W.J. Cook, J. Habash, J.R. Helliwell, J.D. Stoeckler, R.E. Parks Jr., S.-F. Chen, C.E. Bugg, Three-dimensional structure of human erythrocytic purine nucleoside phosphorylase at 3.2 Å resolution, J. Biol. Chem. 265 (3) (1990) 1812–1820.

[25] A. Fedorov, W. Shi, G.A. Kicska, E.V. Fedorov, P.C. Tyler, R.H. Furneaux, J.C. Hanson, G.J. Gainsford, J.Z. Larese, V.L. Schramm, S.C. Almo, Transition state structure of purine nucleoside phosphorylase and principles of atomic motion in enzymatic catalysis, Biochemistry 40 (2001) 853–860.

[26] C. Mao, W.J. Cook, M. Zhou, A.A. Federov, S.C. Almo, S.E. Ealick, Calf spleen purine nucleoside phosphorylase complexed with substrates and substrates analogues, Biochemistry 37 (1998) 7135–7146.

[27] F. Canduri, L.G.V.L. Teodoro, C.C.B. Lorenzi, V. Hial, R.A.S. Gomes, J. Ruggiero Neto, W.F. de Azevedo Jr., Crystal structure

of human uropepsin at 2.45 Å resolution, Acta Crystallogr. D 57 (2001) 1560–1570.
[28] W.F. De Azevedo Jr., F. Canduri, V. Fadel, L.G.V.L. Teodoro, V. Hial, R.A.S. Gomes, Molecular model for the binary complex of uropepsin and pepstatin, Biochem. Biophys. Res. Commun. 287 (1) (2001) 277–281.
[29] W.F. De Azevedo Jr., F. Canduri, N.J.F. da Silveira, Structural basis for inhibition of cyclin-dependent kinase 9 by flavopiridol, Biochem. Biophys. Res. Commun. 293 (2002) 566–571.
[30] W.F. De Azevedo Jr., J.S. de Oliveira, L.A. Basso, M.S. Palma, J.H. Pereira, F. Canduri, D.S. Santos, Molecular model of Shikimate kinase from *Mycobacterium tuberculosis*, Biochem. Biophys. Res. Commun. 295 (1) (2002) 142–148.
[31] W.F. De Azevedo Jr., R.T. Gaspar, F. Canduri, J.C. Camera, N.J.F. da Silveira, Molecular model of cyclin-dependent kinase 5 complexed with roscovitine, Biochem. Biophys. Res. Commun. 297 (2002) 1154–1158.
[32] S.-H. Kim, U. Schulze-Gahmen, J. Brandsen, W.F. de Azevedo Jr., Structural basis for chemical inhibitor of CDK2, Prog. Cell Cycle Res. 2 (1996) 137–145.
[33] W.F. De Azevedo Jr., H.J. Mueller-Dieckmann, U. Schulze-Gahmen, P.J. Worland, E. Sausville, S.-H. Kim, Structural basis for specificity and potency of a flavonoid inhibitor of human CDK2, a cell cycle kinase, Proc. Natl. Acad. Sci. USA 93 (7) (1996) 2735–2740.
[34] W.F. De Azevedo Jr., S. Leclerc, L. Meijer, L. Havlicek, M. Strnad, S.-H. Kim, Inhibition of cyclin-dependent kinases by purine analogues: crystal structure of human CDK2 complexed with roscovitine, Eur. J. Biochem. 243 (1997) 518–526.
[35] W.F. De Azevedo, R.T. Gaspar, F. Canduri, J.C. Camera, N.J.F. da Silveira, Molecular model of cyclin-dependent kinase 5 complexed with Roscovitine, Biochem. Biophys. Res. Commun. 297 (5) (2002) 1154–1158.
[36] J.A. Montgomery, Purine nucleoside phosphorylase: a target for drug design, Med. Res. Rev. 13 (3) (1993) 209–228.
[37] R.W. Miles, P.C. Tyler, R.H. Furneaux, C.K. Bagdassarian, V.L. Schramm, One-third-the-sites transition-state inhibitors for purine nucleoside phosphorylase, Biochemistry 37 (1998) 8615–8621.
[38] G.A. Kicska, P.C. Tyler, G.B. Evans, R.H. Furneaux, W. Shi, A. Fedorov, A. Lewandowicz, S.M. Cahill, S.C. Almo, V.L. Schramm, Atomic dissection of the hydrogen bond network for transition-state analogue binding to purine nucleoside phosphorylase, Biochemistry 41 (49) (2002) 14489–14498.
[39] A. Nicholls, K. Sharp, B. Honig, Protein folding and association: insights from the interfacial and thermodynamic properties of hydrocarbons, Proteins Struct. Funct. Genet. 11 (1991) 281–296.
[40] P.J. Kraulis, MOLSCRIPT: a program to produce both detailed and schematic plots of proteins, J. Appl. Crystallogr. 24 (1991) 946–950.
[41] E.A. Merritt, D.J. Bacon, Raster3D: Photorealistic Molecular Graphics, Methods Enzymol. 277 (1997) 505–524.